High free-tropospheric Aitken-mode aerosol concentrations buffer cloud droplet concentrations in large-eddy simulations of precipitating stratocumulus

Matthew C. Wyant[1], Christopher S. Bretherton[1,2], Robert Wood[1], Peter N. Blossey[1], Isabel L. McCoy[3,4]

[1]University of Washington, Seattle, WA, USA
[2]Allen Institute for Artificial Intelligence, Seattle, WA, USA
[3]Rosenstiel School of Marine and Atmospheric Science, University of Miami, Miami, FL, USA
[4]University Corporation for Atmospheric Research, Boulder, CO, USA

Key Points:

- A simple two-mode aerosol scheme allows exploration of Aitken effects on aerosol and cloud evolution.
- Aitken aerosols supplement the accumulation mode and can prevent boundary-layer collapse in some cases.
- Scavenging of interstitial aerosol particles by cloud droplets has a strong effect on aerosol evolution.

Corresponding author: Matthew Wyant, mwyant@atmos.washington.edu

Abstract

A new Aitken mode aerosol scheme is developed for a large eddy simulation (LES) model in order to better investigate cloud-aerosol interactions in the marine boundary layer and to study the Aitken buffering hypothesis of McCoy et al. (2021). This scheme extends the single-mode two-moment prognostic aerosol scheme of Berner et al. (2013). Nine prognostic variables represent accumulation and Aitken log-normal aerosol modes in air and droplets as well as 3 gas species.

Scavenging of interstitial aerosol by cloud and rain drops and coagulation of dry aerosol are treated using the scheme described in B13. The scheme includes a simple chemistry model with gas phase H_2SO_4, SO_2, and DMS as prognostic variables to capture basic influences of sulfur chemistry on the model aerosols. Primary nucleation of H_2SO_4 aerosol particles from gas-phase H_2SO_4 is neglected.

A deep, precipitating stratocumulus case (VOCALS RF06) is used to test the new scheme. The presence of the Aitken mode aerosol increases the cloud droplet concentration through activation of the larger Aitken particles and delays the creation of an ultraclean, strongly precipitating cumulus state. Scavenging of dry accumulation and Aitken particles by cloud and precipitation droplets accelerates the collapse. Increasing either the above-inversion Aitken concentration or the surface Aitken flux increases the Aitken population in the boundary layer and prevents the transition to an ultraclean state.

Plain Language Summary

Aerosols can have large effects on low-level oceanic clouds, and cloud processes strongly affect aerosols as well. Both aerosols and clouds are a major source of uncertainty in climate projections. A standard tool for studying low altitude ocean clouds and their interactions with aerosols is large-eddy-simulation (LES), but this tool can be very computationally expensive when aerosols of many different sizes are included, which can restrict the geographic coverage, the model resolution, and the time extent of model simulations.

We present a new numerical framework for LES that allows treatment of two size categories of aerosols and their interactions with clouds in a relatively simple and inexpensive manner. We use this framework and perform a wide range of experiments where

aerosol number, properties, and physics are varied in a 10-day simulation of low clouds in a small region over the Southeast Pacific Ocean. Our experiments show that small aerosols can have large effects on low cloud survival in some circumstances.

1 Introduction

Cloud-aerosol interactions can play an important role in the cloud cover and evolution of the marine boundary layer. Ship tracks and pockets of open cells (POCs) demonstrate the connections between aerosol concentrations and cloud properties and dynamics (e.g. Durkee et al., 2000; Wood et al. , 2011).

In the remote marine boundary layer away from anthropogenic and natural land aerosol sources, it has often been thought that cloud condensation nucleus concentrations are generally low, rendering cloudy boundary layer processes especially susceptible to aerosol perturbations (Platnick and Twomey, 1994). However, over the Southern Ocean during summer, boundary-layer cloud droplet number concentrations are typically 50-100 cm^{-3}, comparable to other ocean regions closer to continental outflows (McCoy, D. et al., 2018; McCoy et al., 2020). McCoy et al. (2021) recently proposed that high concentrations of Aitken aerosols nucleated in the free troposphere by synoptic uplift of marine biogenic sulfur-containing gases may buffer the accumulation mode in the Southern Ocean boundary layers. Once brought into the BL (Covert et al., 1996), these Aitken particles act as the main source for growing SO CCN (e.g. Quinn et al., 2017; Raes, 1995). Additionally, it is hypothesized that this large reservoir of Aitken particles can be activated when precipitation removal leads to increased cloud base peak supersaturations, acting to sustain cloud droplet concentrations and therefore help to slow the formation of drizzle or rain (McCoy et al., 2021). While the SO is an extreme example of this buffering mechanism due to the large quantity and continuous creation of FT Aitken particles, it is likely that other ocean regions that experience sufficient quantities of Aitken aerosols may also experience these effects (e.g. the NEA Sanchez et al., 2018; Zheng et al., 2018).

Aerosol and related chemical processes have long been represented in regional models by sorting aerosols into size categories in sectional or bin models (e.g., WRF-CHEM with MOSAIC, Zaveri et al., 2008). These schemes can include dozens of chemical and

large numbers of bins or modes. Bin schemes have also been developed for LES and used to simulate stratocumulus clouds (e.g. Ovchinnikov and Easter, 2010; Tonttila et al., 2017).

To avoid the large computational costs of these schemes, especially in relatively high resolution LES or CRM models, modal schemes with a small number of modes can be used. This approach was used by Ekman et al. (2006) to study processing of Aitken aerosols in cumulus convection. Kazil et al. (2011) used a modal scheme to investigate Aitken aerosols and the role of gas-to-particle conversion in a study of marine stratocumulus over the SE Pacific Ocean.

In this paper, we interactively couple a large-eddy simulation (LES) of a cloud-topped marine boundary layer with simple representations of Aitken and accumulation mode aerosols and sulfur chemistry, and we use this aerosol-coupled LES to demonstrate the plausibility of the McCoy et al. (2021) 'Aitken buffering' hypothesis in an idealized subtropical environment.

Specifically, we couple the System for Atmospheric Modeling (SAM, Khairoutdinov and Randall, 2003) LES, including two-moment warm-cloud microphysics, with a two-mode, two-moment aerosol scheme, together with minimalist marine sulfur chemistry distilled from the CESM Modal Aerosol Model 3, MAM-3 (Liu et al., 2012). Our methodology builds on the one-mode aerosol scheme of Berner et al. (2013), hereafter B13, designed for SAM.

We simulate an idealized case based on a stratocumulus topped boundary layer in an environment favorable to the formation of pockets of open cells (POCs) and sensitive to aerosol concentrations. The case is similar to that of B13 and Kazil et al. (2011) and is based on Research Flight 6 (RF06) of the VAMOS Ocean Cloud Atmosphere Land Study (VOCALS) on Oct. 28, 2008 (Wood et al., 2011). In B13's simulations, the stratocumulus boundary layer collapsed after several days into a shallow, low-albedo ultraclean state, due to aerosol-cloud-precipitation feedback modulated by scavenging of accumulation aerosol. We use our two-mode scheme to study the impact of Aitken aerosols on this collapsing case at higher spatial resolution and over longer time scales than Kazil et al. (2011).

The paper is structured as follows: Section 2 describes the model physics including the two-mode scheme and chemistry model. In section 3 the idealized VOCALS case

study is described and the model setup details for all experiments are summarized. Section 4 presents the experimental results. Discussion and conclusions are presented in Section 5.

2 Model Description

We use SAM version 6.10, including the Rapid Radiative Transfer Model (RRTM, Mlawer et al., 1997) with no direct radiative effects of aerosol. SAM uses centered-differenced momentum advection, and we selected the scalar advection scheme of Yamaguchi et al. (2011). Subgrid fluxes are computed with SAM's 1.5-order TKE scheme.

Our modal approach to aerosol representation is fundamentally based on the work of Whitby et al. (1991). At each grid point, each aerosol mode is represented by lognormal distribution of sizes which can be characterized by two parameters, the geometric mean dry diameter, D_m, and a fixed geometric standard deviation, σ_g. As in B13, we predict the dry aerosol mass mixing ratio, q (kg kg^{-1}), and number concentration, N (mg^{-1}), to characterize each mode. Together q, N, and σ_g determine D_m at each grid point for each mode. The two modes, which we will call 'Aitken' and 'accumulation' will in general overlap with the large tail of the Aitken mode exceeding the size of the small tail of the accumulation mode. To avoid ambiguity, comparisons with observed aerosol number concentrations should be made using fixed size ranges and summations of both modes in each range.

Our aerosol scheme is designed for simulations of the remote marine boundary layer. Our implementation of the Aitken-mode builds on B13's implementation of the accumulation mode, which in turn is built on the bulk 2-moment microphysics scheme of Morrison and Grabowski (2008). As in B13, we assume all aerosol is soluble with the dry density and hygroscopicity of ammonium sulfate, and three categories of accumulation mode aerosol are tracked: interstitial aerosol (q_{ad}, N_{ad}), cloud-droplet-borne aerosol (q_{aw}, N_c), and rain-drop-borne aerosol (q_{ar}, N_r). Cloud drop (N_c) and rain drop (N_r) number concentrations are already accounted for in the existing microphysical scheme, leaving four additional variables (q_{ad}, q_{aw}, q_{ar}, and N_{ad}) to represent accumulation mode aerosol properties. Upon collision and coalescence of cloud droplets and rain droplets, the dissolved aerosol merges with no change in dry aerosol mass. When a cloud droplet or rain drop evaporates, a single aerosol particle is produced. In this way the prognostic number con-

centrations of cloud droplets (N_c) and rain droplets (N_r) implicitly contain aerosol number information. In B13, the assumption of a lognormal distribution primarily affects aerosol activation and scavenging.

In a departure from B13, we define a new prognostic variable q_{acc} as the sum of the interstitial accumulation mode aerosol mass q_{ad} and cloud-borne accumulation mode aerosol mass q_{aw}. The lognormal accumulation number distribution with mass q_{acc} and number N_c+N_{ad} is partitioned by assuming all aerosols above a dividing size are cloud borne and below that size are interstitial. The dividing size is calculated from the interstitial number fraction $N_{ad}/(N_c$+$N_{ad})$. The masses q_{aw} and q_{ad} are defined as the integrated mass above and below this size, respectively, and are now diagnostic, and not prognostic, variables. The number concentrations of each category, N_c and N_{ad}, remain as separate prognostic variables.

To track Aitken-mode aerosol as a separate log-normal mode at each grid point, we add two prognostic variables, q_{ait} and N_{ait}, for mass mixing ratio and number, respectively. Rather than having the Aitken mode represent a fixed aerosol size range, a novel scheme discussed in section 2.1 is implemented to transfer Aitken aerosols to the accumulation mode so that the Aitken mode is predominantly composed of aerosol that has never been activated, while the accumulation mode is predominantly composed of larger aerosol that has been activated and cloud-processed.

To complete the specification of the log-normal modal distributions, we assume fixed geometric standard deviations σ_g of 1.4 for Aitken aerosols and 1.6 for accumulation mode aerosols. These widths are representative of observed marine-boundary layer size distributions in our VOCALS RF06 case (e.g. Allen et al. (2011)). The coarse mode is not explicitly treated, but its influence on droplet activation is parameterized as described below.

In our scheme, the lognormal shapes of the distributions affect not only activation and scavenging, but also coagulation and aerosol chemistry. We include the scavenging of interstitial aerosol by cloud droplets and rain drops as in B13, extending their treatment to include scavenging of Aitken mode particles. For this purpose, the size of both accumulation and Aitken interstitial aerosol particles is adjusted for equilibrium uptake of water vapor both below and within cloud.

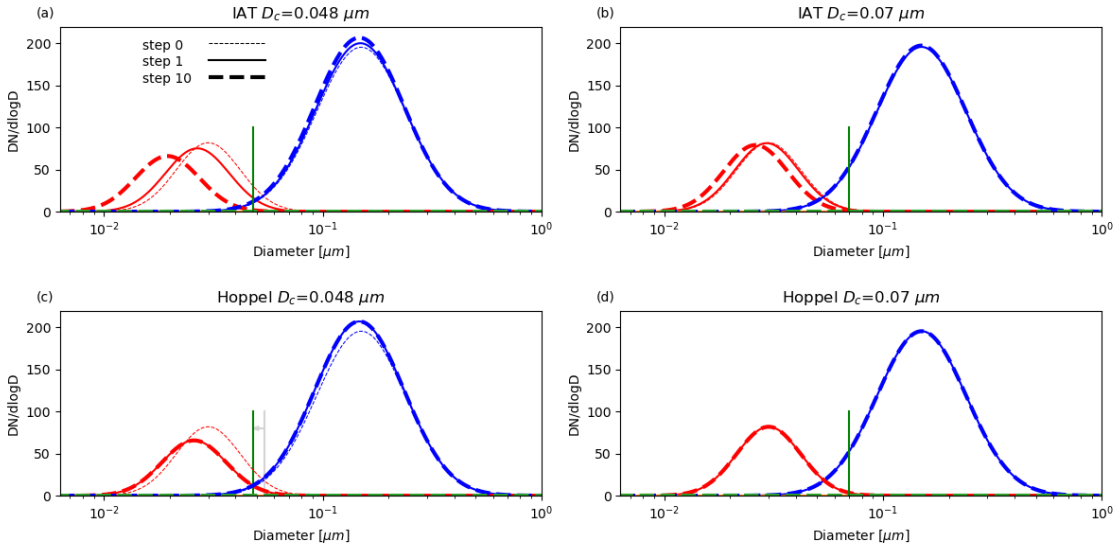

Figure 1. Examples of Aitken transfer schemes for critical diameters D_c (vertical green lines) of 0.048 μm and 0.07 μm on the left and right panels, respectively. Distributions are compared for an initial time (dashed lines), after one time step (solid lines), and after 10 time steps (thick dashed lines). The top panels, (a) and (b), use instantaneous transfer (IAT) and the bottom panels, (c) and (d) use the Hoppel transfer scheme. In (c) the gray line shows the initial Hoppel diameter D_h and the gray arrow shows the resulting shift to a smaller D_h which matches D_c after a single transfer step.

For this study interstitial aerosol coagulation processes are included with a widely used modal formulation (Binkowski and Shankar, 1995; Whitby et al., 1991). We treat both coagulation of particles between modes and within the Aitken mode. Somewhat significant in our MBL simulations is Brownian coagulation of interstitial accumulation-mode and Aitken-mode particles, which transfers Aitken particles onto existing accumulation-mode particles and reduces the Aitken number concentration, especially affecting smaller Aitken particles. Of lesser importance is coagulation within the Aitken mode, which takes several days to substantially increase the mean diameter of the Aitken mode under remote marine conditions.

The conservation equations for aerosol number and mass in this scheme are specified in the Appendix.

2.1 Transfer of activated aerosol from Aitken to accumulation modes

Aerosol activation follows the multi-mode activation scheme of Abdul-Razzak and Ghan (2000), hereafter referred to as ARG, which prescribes activation for each aerosol

mode in a saturated updraft. The ARG scheme requires the aerosol modes to have lognormal size distributions, which dictated our decision to use overlapping Aitken and accumulation modes rather than non-overlapping, truncated size distributions. In saturated updrafts, the ARG scheme uses the aerosol distributions, hygroscopicity and updraft speed to compute a peak supersaturation. For simplicity, we assume in this work that all Aitken and accumulation mode aerosols have the same hygroscopicity and hence the same threshold diameter D_c for the given maximum supersaturation. Both Aitken and accumulation aerosols above this threshold are assumed to be activated. Our approach could be generalized to multiple externally-mixed aerosol types.

Our initial naive approach to modal transfer was to instantaneously transfer any activated aerosols in the large-diameter tail of the Aitken mode into the accumulation mode at each model time step as in Figure 1a-b; we call this instantaneous activation transfer (IAT). In reality, smaller Aitken aerosols would then have to gradually grow or coalesce to fill in this tail. In the model, however, the Aitken mode is always assumed to be lognormal. A new large-diameter tail is reconstituted at the next time step from the updated Aitken mass and number concentration and can be immediately activated. This process induces overly efficient transfer from the Aitken to the accumulation mode, which artificially decreases the Aitken modal size and number concentration. In the figure, the same transfer process is applied over 10 time steps, comparable to the number of steps the transfer would be applied to an updraft of 0.25 ms^{-1} at cloud-base level (corresponding to critical diameter $D_c = 0.048\mu m$ in Figure 1a) as air is vertically advected through one third of single grid level. The size of the Aitken mode is significantly reduced, especially in Fig. 1a which has a lower D_c than Fig. 1b. Small Aitken aerosols are also more vulnerable to in-cloud Brownian diffusion loss, further lowering the simulated Aitken number concentration. Within hours to days, these processes lead to an equilibrated Aitken modal size and number concentration that are unrealistically small.

To avoid these issues, we have implemented a novel modal transfer scheme that addresses this artifact of the assumption of lognormal aerosol modes while still accounting for all activated aerosol in a single way and maintaining a crossover from Aitken-dominated to accumulation-dominated aerosol at a physically reasonable diameter. A first design goal is to minimize the artificial effect (created by the lognormal distribution shape assumption) of large-diameter Aitken activation on the smaller-diameter part of the Aitken size distribution. This is achieved by retaining the activated Aitken aerosol in the Aitken

mode mass and number instead of moving it to the accumulation mode, except as part of a rarer model transfer process to be described below. Smaller accumulation-mode aerosols stand in for these activated Aitken aerosols as part of the activated number N_c and mass q_{aw}.

What matters physically is the overall aerosol size distribution formed by the superposition of the lognormal Aitken and accumulation modes. In any fluid parcel circulating through a cloud-topped boundary layer, this distribution can be divided into smaller-diameter particles that have never been activated into droplets, and larger-diameter particles that have been activated and cloud-processed at some time. The observed aerosol size distribution in such boundary layers commonly exhibits a 'Hoppel minimum' (Hoppel et al., 1990) in the number concentration that is interpreted as the dividing point of this distribution. In our setting, we define a Hoppel diameter D_H as the diameter at which the number concentration of accumulation and Aitken mode aerosols coincide, i.e., $N_{acc}(D_H) = N_{ait}(D_H)$. Typically, D_H is close to a local Hoppel-like minimum of the aerosol size distribution, as can be visualized from the cartoon by mentally adding the solid red and blue curves in Figure 1.

Our second design goal is to ensure that, after activation, the overall aerosol size distribution reflects this observed characteristic. This is accomplished using a modal transfer mechanism that we call 'Hoppel transfer', which only occurs in cloudy updrafts, and in which the critical diameter D_c for activation diagnosed by the ARG scheme in the Morrison microphysics plays a key role. Hoppel transfer is implemented as follows. If the critical diameter D_c is smaller than the Hoppel diameter D_H (i.e., the Aitken number is larger than the accumulation number at D_c), we transfer just enough Aitken particles of size D_c from the Aitken to the accumulation mode so that $D_H = D_c$ (Figure 1c). With this approach, computing the required transfer is very simple and efficient, and after one time step, no further transfer occurs when D_c is constant. In regions of cloud droplet activation where $D_c > D_H$ (as might occur in a weak updraft, Fig. 1d), the Hoppel transfer is inactive. In the absence of other processes that modify the aerosol, the diagnosed one-way transfer process keeps the Hoppel diameter from exceeding the smallest D_c activated in saturated ascent of the air parcel.

Large sea-salt aerosol particles are represented by the inclusion of an additional specified coarse mode when computing maximum supersaturation in the ARG scheme. This

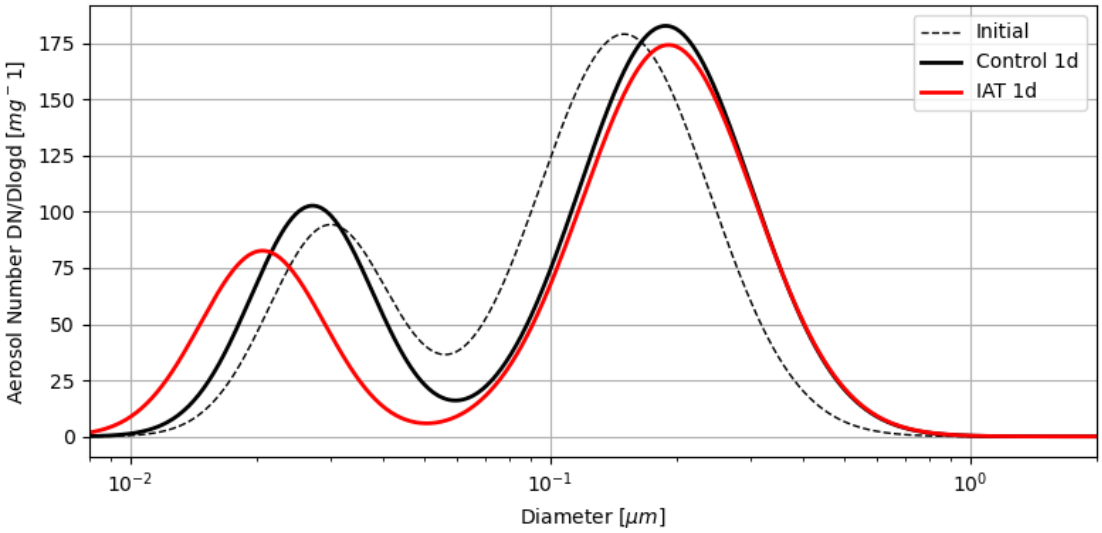

Figure 2. Comparison of Mean BL aerosol size distributions for Control using Hoppel transfer (solid black) and Instantaneous activation transfer (red) simulations after 1 day. Dashed black line shows the initial size distribution for both simulations.

mode is assumed to have a 2.6 μm modal diameter, σ_g of 2.5, a typical sea-salt hygroscopicity of 1.1 (Zieger et al., 2017), and 0.13 mg^{-1} number concentration, and typically reduces ARG maximum supersaturations by about 5%. Wind-speed dependence of this large aerosol mode is neglected for simplicity in this work, but could easily be added for enhanced realism.

Fig. 2 illustrates the sensitivity of the Aitken size distribution to the modal transfer method after one day of simulation. The dashed and solid black lines show, respectively, boundary-layer averaged aerosol size distributions at the start and one day into a Control simulation, fully described below, that uses the Hoppel transfer algorithm. After one day, there is a Hoppel minimum at about 50 μm diameter, and the Aitken modal diameter is nearly 30 μm. The red line shows corresponding results at one day from a otherwise identically configured and initialized simulation with our naive approach, instantaneous activation transfer or IAT. In the IAT simulation, the Aitken mode rapidly develops a smaller modal diameter of 20 μm and a 25 % lower overall number concentration than in the Control simulation.

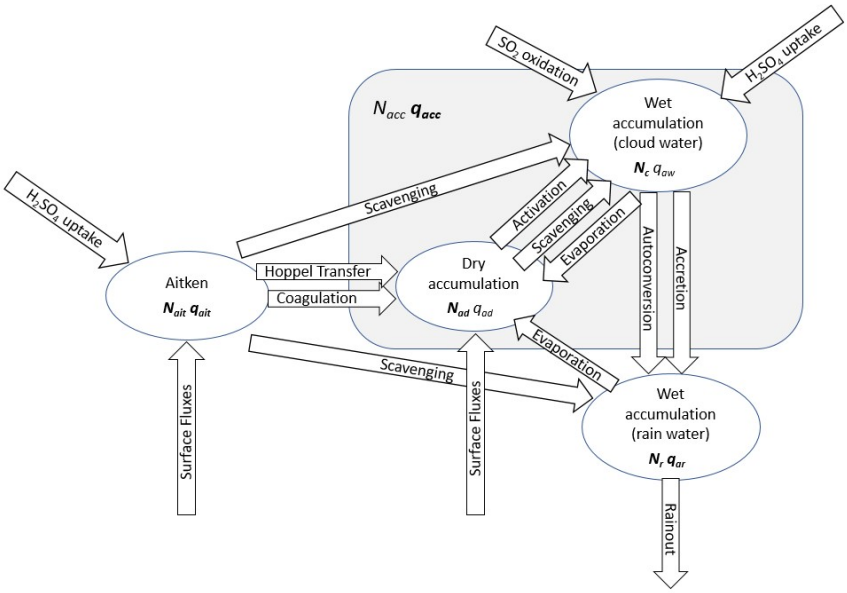

Figure 3. Aerosol-scheme categories and boundary-layer processes that affect them. Prognostic variables are shown in bold font.

2.2 Summary of processes transferring number and mass between aerosol categories

Figure 3 is a schematic of the processes (arrows) that affect the aerosol categories (ovals). All of the processes moving aerosol between categories conserve total aerosol mass. However, total aerosol number is reduced by autoconversion, accretion, and interstitial scavenging. There are three direct pathways for the loss of particles from the Aitken mode to the accumulation mode: scavenging, coagulation, and activation transfer.

Scavenging of Aitken aerosol by cloud droplets or raindrops moves the Aitken particle's mass into the accumulation mode because the scavenging drops are all assumed to contain accumulation particles, and upon evaporation all aerosol mass is kept in the accumulation mode. This process is also a sink of Aitken number concentration.

Coagulation between Aitken and interstitial accumulation aerosols is assumed to increase accumulation mode mass at the expense of Aitken mass and number concentration. Aitken-Aitken dry coagulation depletes Aitken number concentration while increasing Aitken size over a timescale of days. Coagulation between interstitial accumulation mode particles is neglected. In the experiments presented here, coagulation is sus-

pended in the free troposphere above 1800m so that nearly constant aerosol properties are maintained above the inversion.

All microphysical processes that affect accumulation mode aerosol mass in rain droplets are assumed to affect it in proportion to the ratio of aerosol mass to water mass, following B13 and Flossmann et al. (1985).

2.3 Surface Aerosol Fluxes

Surface fluxes of aerosol are horizontally uniform and are specified based on the sea-salt aerosol flux parameterization of Clarke et al. (2006) and dependent on the domain-mean wind speed near the surface. The number flux of surface aerosol ($\mathrm{m^2 s^{-1}}$) for each mode is

$$F_{Naero} = C_S W U_{10}^{3.41}, \tag{1}$$

where $W = 3.84 \times 10^{-6}$ and U_{10} is the 10-m neutral windspeed ($\mathrm{m\,s^{-1}}$) calculated using the winds at the lowest model level. For our experiments here the coefficients C_S for accumulation and Aitken modes are each set to 4.37×10^7. This gives a total number flux of accumulation plus Aitken modes very close to the total number flux in Clarke et al. (2006). We also specify a fixed diameter for emissions of each mode. Like Clarke et al. (2006) and B13, our mass flux parameterization has an identical wind-speed dependence as the number flux. Because of this and our Gaussian modal treatment, for each mode the surface aerosol mass flux ($\mathrm{kg\,m^{-2}\,s^{-1}}$) is uniquely determined by the number flux together with the specified modal diameter D_m:

$$F_{qa} = \frac{\pi}{6} D_m^3 \rho_a \exp\left(\frac{9}{2} \log^2 \sigma_g\right) F_{Naero}. \tag{2}$$

Here ρ_a is the aerosol density. For our simulations here we choose $D_{m,accum} = 150\,\mathrm{nm}$ and $D_{m,ait} = 30\,\mathrm{nm}$; these are also used to specify the initial size distributions of the two aerosol modes. Figure 4 shows a comparison of aerosol-flux size distributions for our 2-mode approximation with the Clarke formulation, all using a wind speed of $U_{10} = 9.0\,\mathrm{ms^{-1}}$.

2.4 Model Chemistry

We include a simple scheme to treat basic sulfur chemistry relevant to aerosols, following the approach of the CESM MAM-3 (Liu et al., 2012). We include three prognos-

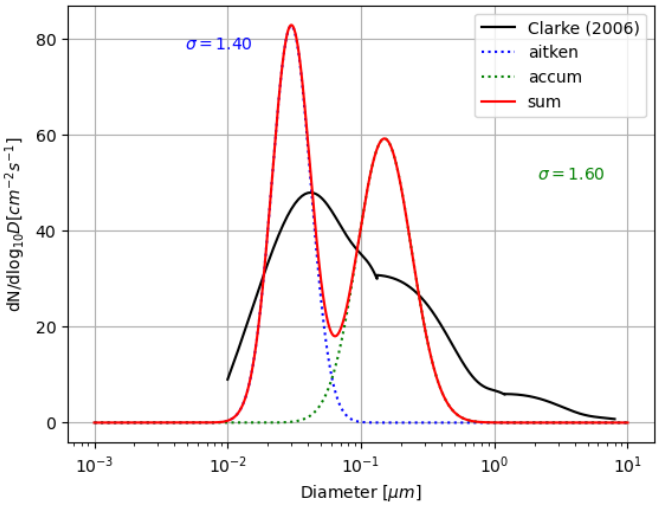

Figure 4. Parameterized surface aerosol number flux parameterizations given a wind speed $U_{10} = 9$ m s^{-1} for Clarke et al. (2006) (solid black), and for the two-mode parameterization used here (solid red). Individual modes are plotted as dotted lines.

tic variables for tropospheric gases: DMS, SO_2, and H_2SO_4. We also account for processes that increase the aerosol sulfate mass though aqueous chemistry and uptake of H_2SO_4 by aerosol particles.

We include the production of SO_2 due to the reaction of DMS with OH and NO_3, the loss of SO_2 due to reaction with OH, and the reaction of SO_2 with OH to produce H_2SO_4. These reactions have the following rate equations:

$$\frac{d[\mathrm{DMS}]}{dt} = -r_1[\mathrm{OH}][\mathrm{DMS}] - r_2[\mathrm{OH}][\mathrm{DMS}] - r_3[\mathrm{NO_3}][\mathrm{DMS}] \tag{3}$$

$$\frac{d[\mathrm{SO_2}]}{dt} = r_1[\mathrm{OH}][\mathrm{DMS}] + \frac{1}{2}r_2[\mathrm{OH}][\mathrm{DMS}] + r_3[\mathrm{NO_3}][\mathrm{DMS}] - r_4[\mathrm{OH}][\mathrm{SO_2}] \tag{4}$$

$$\frac{d[\mathrm{H_2SO_4}]}{dt} = r_4[\mathrm{OH}][\mathrm{SO_2}], \tag{5}$$

where all concentrations denoted by [ ] have units of molecules cm^{-3}, concentrations of OH and NO_3 are specified constants and uniform, and r_1,r_2,r_3, and r_4 are temperature dependent rate constants from MAM-3.

We represent aqueous production of sulfate mass in cloud drops due to oxidation of SO_2 by H_2O_2 following the GEOS-Chem model (Bey et al., 2001). Dissolved aqueous concentrations of SO_2 and H_2O_2 are determined using Henry's law from gas concentrations. The resulting equation for sulfate production can be expressed in terms of gas concentrations as

$$\frac{d\mathrm{SO_4}(aq)}{dt} = K_{aqox}[\mathrm{SO_2}][\mathrm{H_2O_2}], \tag{6}$$

where the rate constant K_{aqox} depends on temperature and pH, and includes Henry's constants for SO_2 and H_2O_2. We specify a constant droplet pH of 5 representative of remote ocean regions.

Aerosol sulfate mass can be increased by condensation of H_2SO_4 onto cloud drops and aerosol particles. This is treated following MAM-3 as an irreversible process using the diffusion equation

$$\frac{d\mathrm{H_2SO_4}(g)}{dt} = 4\pi r D_{\mathrm{H_2SO_4}} \tag{7}$$

where r is the cloud drop or aerosol radius and $D_{\mathrm{H_2SO_4}}$ is the gas diffusivity of H_2SO_4. For uptake on aerosols, r is adjusted for ambient relative humidity.

2.5 DMS Fluxes

Tropospheric DMS is replenished by surface fluxes using the following simple bulk formulation of Nightingale et al. (1999):

$$F_{\mathrm{DMS}} = 10^{-7}(7.5U_{10} + 5U_{10}^2)C, \tag{8}$$

where C is the specified ocean surface DMS concentration [mol m^{-3}] and the DMS flux F_{DMS} has units of mol $m^{-2}s^{-1}$. For the experiments described below, we follow Wyant et al. (2015) and use $C = 2.8 \times 10^6$ mol m^{-3} based on VOCALS regional measurements.

2.6 Neglected processes

In this first study with this new scheme, several processes are neglected for simplicity. We do not simulate new particle formation or dry deposition of aerosol. In addition, direct radiative effects of aerosols are not included in the simulations.

3 Experiment Description

We simulate an idealized version of the VOCALS RF06 case with an environmental setup that is nearly identical to that of B13. The model and environmental simulation parameters are summarized in Table 1. We use a vertically uniform geostrophic wind. The large-scale divergence is assumed to be steady and uniform up to 3km with a value of 3.33×10^{-6} s^{-1}, the same as used in the majority of simulations in B13. This produces a subsidence rate of 5.0 mm s^{-1} at 1500 m. This subsidence rate is stronger than the observed value of 2 mm s^{-1} (Wood et al., 2011) but helps maintain a steady MBL depth in our simulations. We also apply constant, diurnally averaged insolation. Temperature and moisture profiles more than 150 m above the inversion are nudged towards initial values with a relaxation timescale of one hour. Our simulations have 125 m horizontal grid spacing and a variable vertical grid spacing with a total of 384 vertical levels: 30 m spacing near the surface, 5m spacing up to 1500 m with rapidly coarsening resolution and 41 levels above 5000 m.

A summary of all the experiments is presented in Table 2.

4 Experiment Results

4.1 Control Case

Our control case is broadly similar to the 3D control case presented in B13. It differs from B13 in its reduced initial BL and FT accumulation mode concentrations and in the inclusion of an Aitken mode with initial number concentrations of 30 mg^{-1} in the boundary layer and 100 mg^{-1} in the FT.

The boundary layer structure and cloud cover change dramatically over the course of the simulation, evident in the evolution of horizontally-averaged cloud water (Fig. 5 (a)). After 4 1/2 days the cloud-topped boundary layer collapses due to a steady depletion of boundary layer accumulation model aerosol (Fig. 5) into a shallower "ultra-clean"

Table 1. VOCALS RF06 Control Simulation Parameters. Some initialization values are separately specified for the marine boundary layer (MBL) and free troposphere (FT).

Parameter	Symbol	Value
	Constants	
SST		291.15 K
geostrophic wind	U_g	2.33 m s^{-1}
geostrophic wind	V_g	11.97 m s^{-1}
large-scale divergence	D	3.33×10^{-6} s^{-1}
horiz. grid size	$\Delta x, \Delta y$	125 m
vert. grid size (min)	Δz	5 m
horiz. domain size		8 km x 8 km
time step	Δt	0.75 s
$[NO_3]$		5.0×10^{-11} kg kg^{-1}
$[H_2O_2]$		7.0×10^{-10} kg kg^{-1}
$[OH]$		5.0×10^{6} molecules cm^{-3}
pH		5
	Initial Conditions	
MBL accumulation conc.	N_{ad}	80 mg $^{-1}$
FT accumulation conc.	N_{ad}	40 mg $^{-1}$
accumulation diameter	$D_{m,ad}$	0.15 μm
MBL Aitken conc.	N_{ait}	30 mg $^{-1}$
FT Aitken conc.	N_{ait}	100 mg $^{-1}$
Aitken diameter	$D_{m,ait}$	0.03 μm
Cloud Droplet number	N_d	30 mg $^{-1}$
$[SO_2]$		5.0×10^{-12} kg kg^{-1}
$[H_2SO_4]$		5.0×10^{-14} kg kg^{-1}
$[DMS]$ MBL		10.0×10^{-10} kg kg^{-1}
$[DMS]$ FT		0.0 kg kg^{-1}

Table 2. Experiment details. Initial boundary layer and free tropospheric aerosol number concentrations are given in mg^{-1}. FT Aerosol number and mass do not change much during these experiments, in part because coagulation is suppressed above 1800 m.

Run Name	BL Aitken	FT Aitken	Other Condition
Control	30	100	
FT1000	30	1000	
FT30	30	30	
Surfx10	30	100	surface aerosol flux × 10
BL1000	1000	100	
NoScav	30	100	no interstitial scavenging
NoChem	30	100	no chemistry
WideAit	30	100	$\sigma_g = 1.8$ for Aitken
IAT	30	100	Aitken transfer on activation only

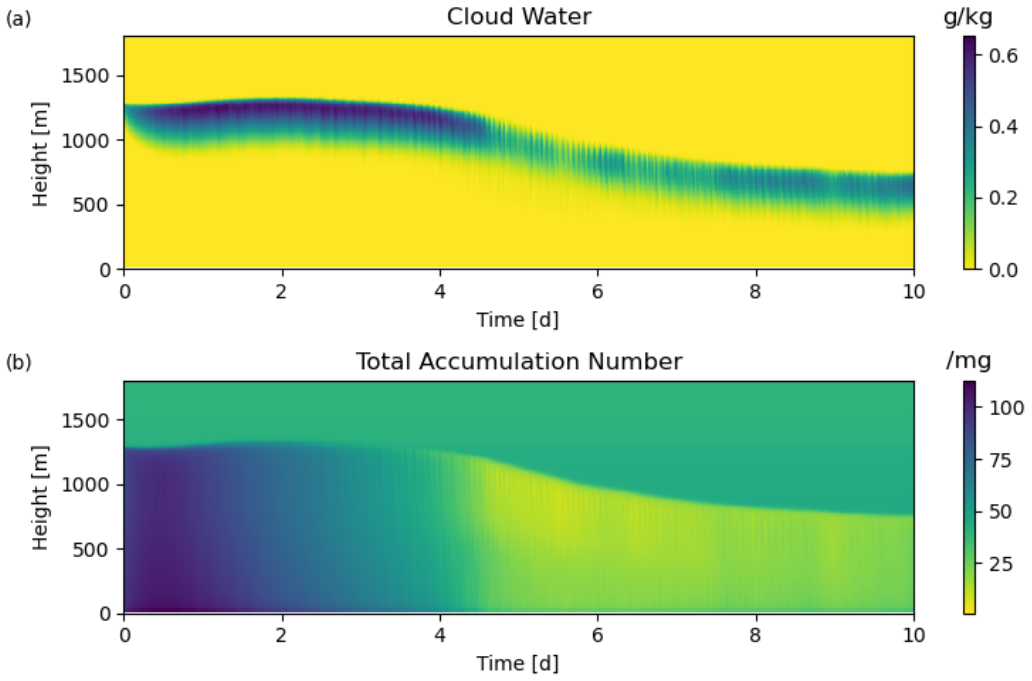

Figure 5. (a) Mean simulated cloud water and (b) total accumulation aerosol concentration in the Control simulation.

BL. This collapse, also described in B13, is caused by a feedback between aerosol concentration, droplet number concentration, and precipitation.

This transformation is documented in more detail in the domain mean soundings and statistics of Fig. 6. The BL initially is 1300m deep and well-mixed with a strong 13 K temperature inversion and a very strong gradient of moisture across the inversion. Over the first 48 hours, the boundary layer deepens by about 50 m and the cloud thickens to produce a relatively steady LWP of about 150 g m^{-2}. This cloud water persists through day 4, though the cloud-top slowly sinks. At day 4.5 the cloud begins rapidly thinning with a sharp reduction in cloud liquid water path and cloud fraction. Because of the associated reduction in cloud fraction, cloud-top turbulence, and entrainment, the boundary layer depth steadily lowers. The resulting state has less than half the LWP of the deeper state and shows evidence of decoupling.

The role of aerosols in this collapse is highlighted in the soundings and aerosol properties in Fig. 7. Profiles of BL accumulation aerosol show dramatic loss between simulation start and day 6, after which an ultra clean state is reached with less than 20 mg^{-1} BL number concentrations. Through day 2 the BL Aitken aerosol concentration is main-

tained, largely through entrainment, but after that point the BL Aitken number concentration is depleted strongly as well. Note the vertical slope in FT Aitken number (Fig. 7b) is due to coagulation of subsiding FT Aitken aerosols.

As described in B13, the BL collapse is fundamentally tied to the steady depletion of accumulation-mode aerosol number concentration. The simulated activation fraction of accumulation-mode aerosols is fairly steady at 75–80% before the collapse, so the droplet number concentrations shows a similar steady decline from 67 mg^{-1} at day 0.5 to 32 mg^{-1} at day 4.0 (Figure 7c). Figure 7d shows the rapidly increasing surface precipitation rate from 0.5–4 despite the steady LWP, which accelerates the loss of accumulation-mode aerosols, triggering a strong feedback and the collapse of the boundary layer.

Despite the steady loss in number, the accumulation aerosol mass increases during the first 4.5 days because of increasing modal diameter(Fig. 7e,f) . This steady increase is due to aqueous oxidation and will be discussed further in section 4.3.

The boundary-layer-mean accumulation (excluding rain-borne aerosol) and Aitken number budgets are shown in Figures 8a-b. We can accurately close both budgets: the red budget residual lines are much closer to zero than the dominant sources and sinks. In the accumulation number budget (Figure 8a), the main sources are surface fluxes (black) and transfer of aerosol from the Aitken mode (green). These are countered by a variety of sinks, principally accretion (turquoise), autoconversion (yellow-green), interstitial scavenging (orange), and entrainment (blue). Evaporation (purple) of rainwater producing dry accumulation aerosol in the subcloud layer only slightly counteracts accretion and autoconversion losses. Note that entrainment becomes a weak source after day 4 when the accumulation number concentration becomes lower in the BL than in the FT. When the cloud droplet number concentration decreases and precipitation increases, autoconversion and especially accretion losses increase, particularly after day 3.

The Aitken number budget (Figure 8b) is dominated by a balance between surface (black) and entrainment (blue) sources and losses due to interstitial scavenging (orange) and activation-driven transfer loss (green), which is important initially and after BL collapse. In contrast to the transfer process, interstitial scavenging preferentially removes smaller Aitken particles.

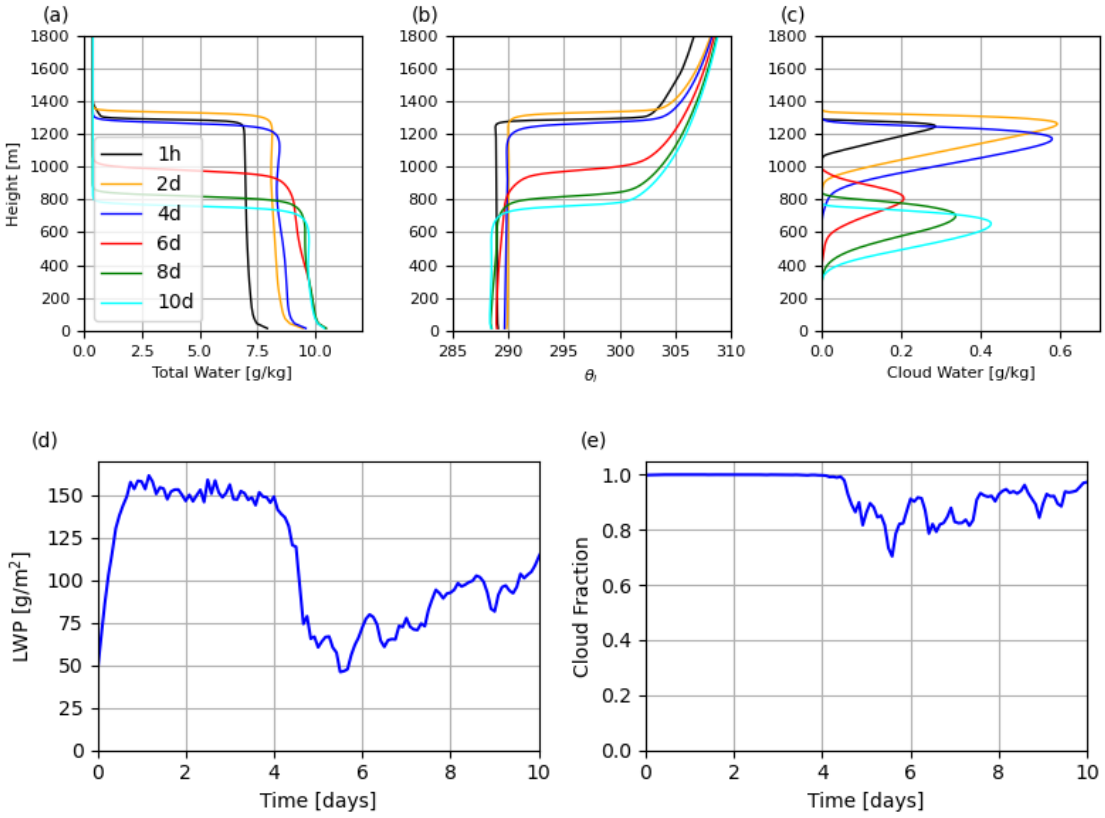

Figure 6. Horizontal-mean vertical profiles at selected times from the Control simulation of (a) total water, (b) liquid water potential temperature, and (c) cloud water. Time series of (d) domain-mean LWP and (e) cloud fraction.

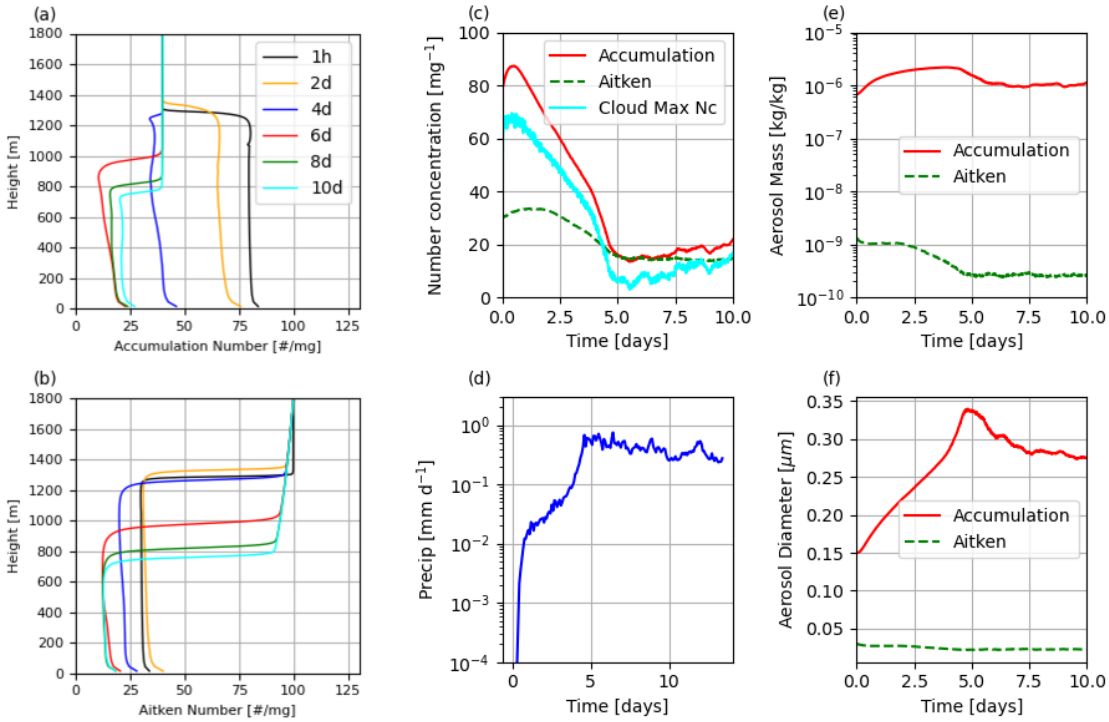

Figure 7. Vertical profiles at selected times from the Control run of (a) total accumulation number concentration, and (b) Aitken number concentration. Time series of (c) BL-mean number concentrations of aerosol and cloud droplets, (d) surface precipitation, (e) BL-mean aerosol mass (e), and (f) modal diameters of the two aerosol modes.

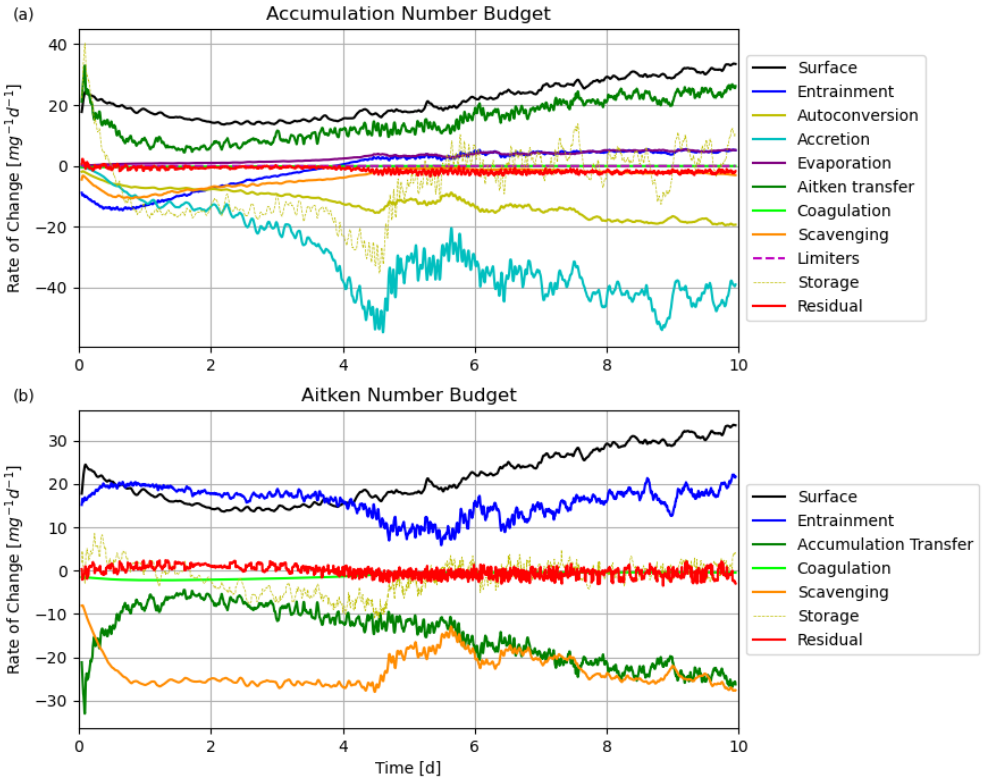

Figure 8. Boundary-layer-mean aerosol number budgets for (a) accumulation mode (excluding rain-water-borne aerosol) and (b) Aitken mode.

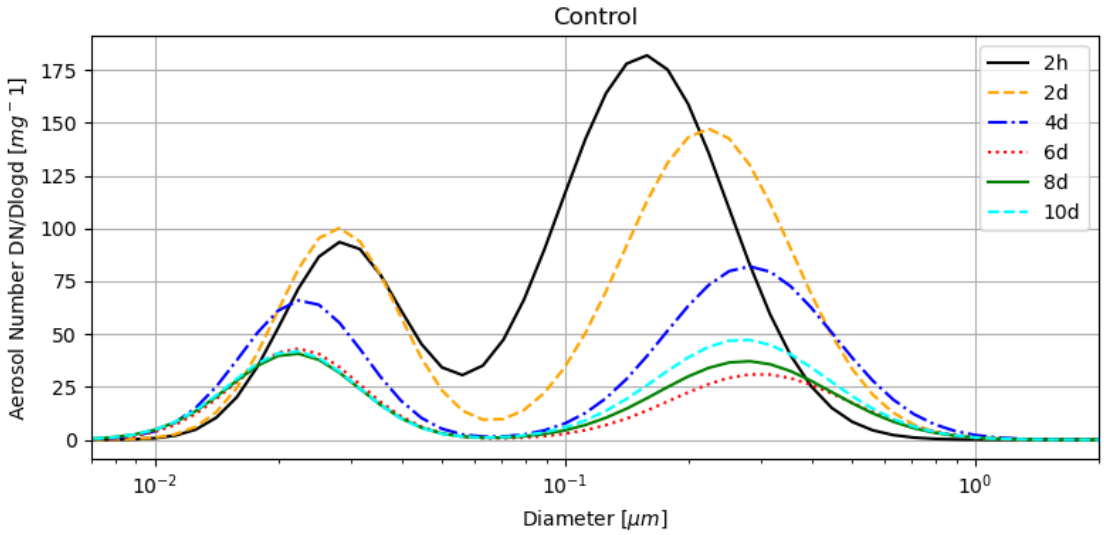

Figure 9. Mean boundary-layer aerosol spectra at 2h, 2d, 4d, 6d, 8d, and 10d of the Control simulation.

Total boundary-layer aerosol number spectra before and after the boundary-layer collapse are shown in Figure 9. At all times plotted, there is a clear Hoppel minimum between the modes, and the modes become more distinct with time. The Aitken aerosol mode moves to a smaller diameter due to the preferential transfer of large Aitken particles. Before collapse the modeled aerosol BL distribution is broadly similar to pre-POC observed aerosol distributions in the VOCALS experiment (e.g. Allen et al., 2011), though with fewer Aitken particles and slightly smaller Aitken sizes. Chemical processes play a relatively minor role in the Aitken aerosol evolution in this case, but cause a substantial increase in the typical size of accumulation mode particles over the first five days, due to aqueous oxidation of SO_2. A NoChem sensitivity simulation will be discussed below.

4.2 Aitken Aerosol Number Perturbations

An important goal is to test whether this model exhibits Aitken buffering and if so, how quickly it acts. We consider a family of 10-day experiments (listed in Table 2) in which Aitken aerosol concentration is perturbed in various ways. In one set of experiments, Aitken number concentration in the free troposphere is changed from the Control value of 100 mg^{-1} to 1000 mg^{-1} (FT1000) or 30 mg^{-1} (FT30). In the Surfx10 experiment, the surface number flux of Aitken aerosols is increased tenfold by scaling C_s

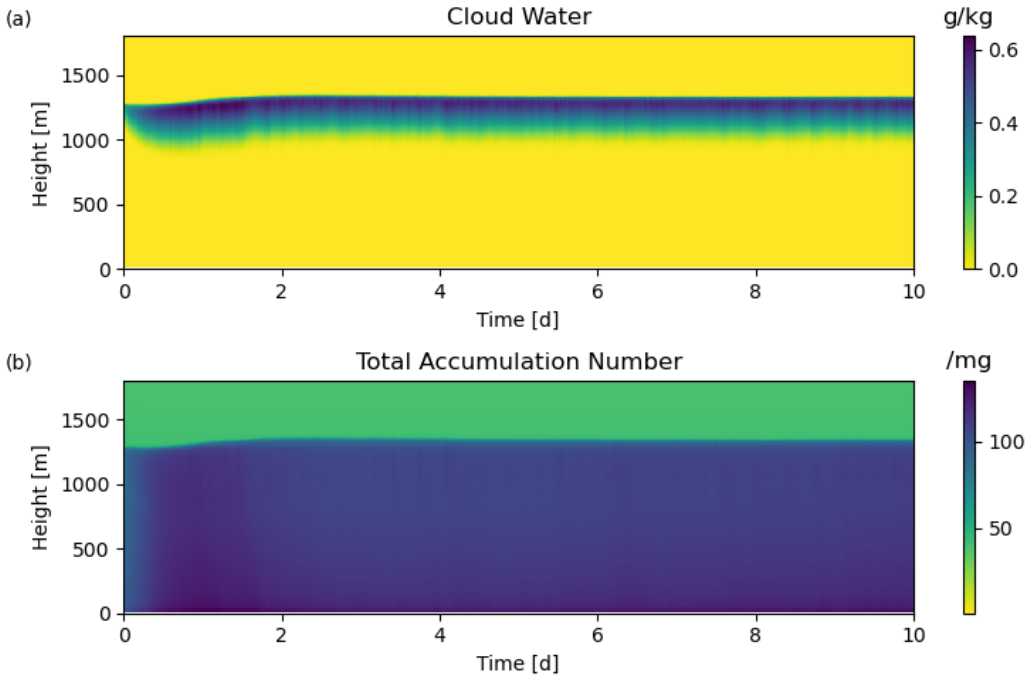

Figure 10. FT1000 Mean simulated cloud water and accumulation aerosol as in Fig.5.

in equation (1) by a factor of 10 for these aerosols. In the BL1000 experiment, the initial Aitken number concentration in the boundary layer is increased from 30 mg^{-1} to 1000 mg^{-1} to test how long BL Aitken perturbations persist when they are not induced by external forcing.

These experiments support the Aitken buffering hypothesis of McCoy et al. (2021). They show that in our model, a large source of Aitken aerosol from either the surface or the free troposphere can stabilize a stratocumulus-capped boundary layer and prevent the formation of simulated pockets of open cells with much lower area-mean albedo. This is illustrated for the FT1000 case in Figure 10. In contrast to Control, FT1000 spins up in the first two days into a deep well-mixed stratocumulus-capped boundary layer with steady-state profiles of cloud water, boundary layer depth, and accumulation aerosol.

Time series of BL-mean statistics from FT1000 and the other Aitken perturbation experiments are compared with Control in Figure 11. For FT1000, a quasi-steady LWP is reached in two days. BL Aitken concentrations reach 225 mg^{-1} as high FT Aitken particle concentrations are entrained into the boundary layer. The largest of these Aitken particles are transferred to the accumulation mode, supporting a steady accumulation

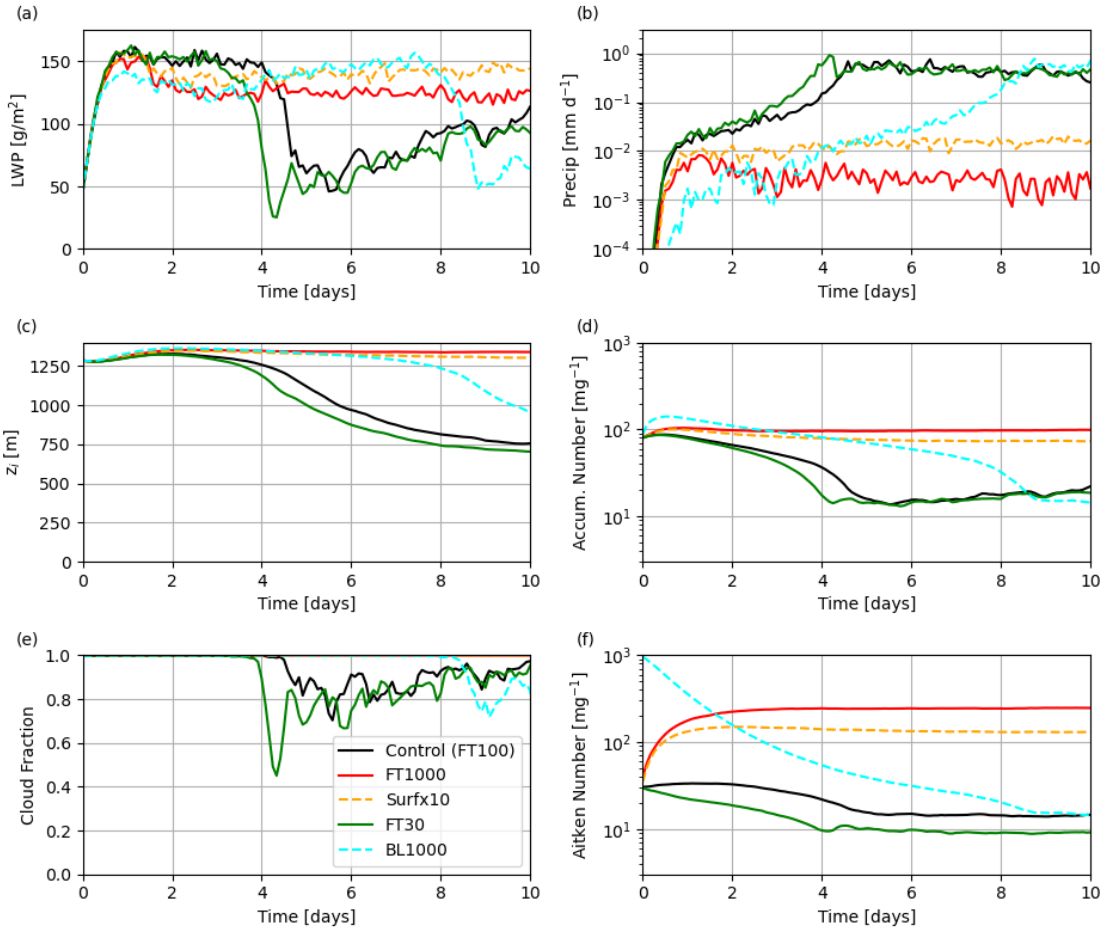

Figure 11. Mean boundary-layer evolution of Control, FT30, FT1000, Surfx10, and BL1000 experiments.

mode concentration of about 100 mg^{-1}. Precipitation stays well below 0.01 mm d^{-1} and no runaway aerosol feedback occurs. The Surfx10 simulation evolves similarly to FT1000.

In the FT30 simulation with reduced FT Aitken aerosols, the BL Aitken concentration declines rapidly in the first four days. This advances the BL collapse by about 15 hours vs. Control, as seen in the evolution of accumulation mode aerosol, inversion height, precipitation and LWP path.

The BL1000 experiment maintains a deep BL and thick stratocumulus layer similar to FT1000 and Surfx10 for about 6 days. However, both Aitken and accumulation number concentrations decrease as the large initial BL Aitken aerosol concentration is consumed. This gradually increases precipitation and initiates BL collapse after 8 days.

We gain further insight into these sensitivity experiments by comparing their aerosol size distributions and number budgets at Day 3, well before the BL collapse in Control (Figure 12). The experiments with positive Aitken perturbations (FT1000, Surfx10, and BL1000) have much larger Aitken concentrations and — supported by transfer from the Aitken mode — substantially larger accumulation concentrations. Compared to Control, the Aitken mode has a size distribution with a larger modal diameter, driven by the surface and FT Aitken reservoirs. The Hoppel minimum is less extreme and moves to a larger diameter. The accumulation mode has reduced modal diameter due to the strong transfer of small Aitken aerosols. In contrast, the FT30 experiment has depleted Aitken and accumulation modes, both with shapes similar to Control. As in Control, the Hoppel minimum in aerosol concentration is broad and pronounced.

Figure 13 compares one-day BL-mean Aitken and accumulation number budgets averaged from day 2.5 to day 3.5. The accumulation number tendency in Control is dominated by autoconversion and accretion losses, countered by sources from surface fluxes and transfer from the Aitken mode. In contrast, the BL accumulation mode concentration in FT1000 is in steady state due to the 20 mg^{-1} d^{-1} transfer from the abundant Aitken mode, more than double the transfer in Control, and reduced precipitation-related autoconversion and accretion losses. In FT1000, accumulation mode number losses due to entrainment and interstitial scavenging are larger than in Control because of the larger accumulation number concentrations, but this is more than made up for by reduced autoconversion and accretion losses.

The Aitken number budget in FT1000 is dominated by the 180 mg^{-1} d^{-1} entrainment source. Brownian scavenging of the smaller Aitken aerosols by cloud droplets is the dominant sink, while the largest entrained Aitken particles are transferred to the accumulation mode.

Comparing the Aitken budget terms of Surfx10 and FT1000 in Fig. 13b for days 2.5-3.5, the surface flux term in Surfx10 is very large but still smaller than the entrainment source term in FT1000. This leads to a slightly weaker transfer to the accumulation mode. Surfx10 has about 35% lower Aitken concentrations than FT1000, and only 10% larger LWP, leading to smaller in-cloud scavenging losses of Aitken aerosols. The accumulation number budgets are fairly similar between the two cases, though Surfx10

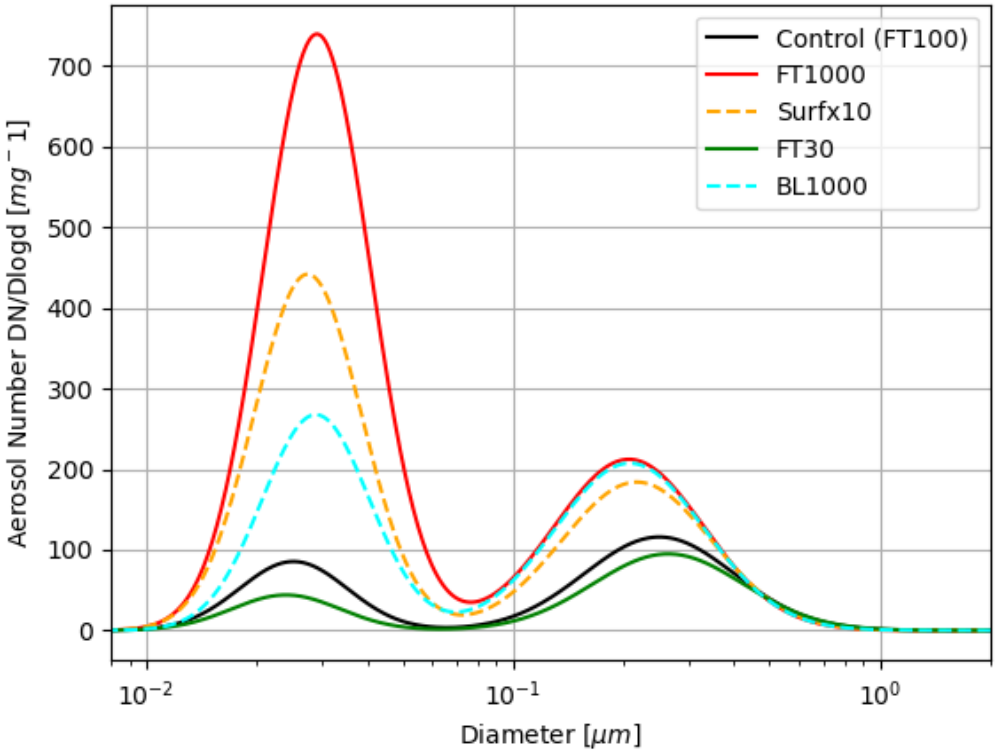

Figure 12. Mean-BL Aerosol distributions for Control and aerosol number perturbation experiments at Day 3.

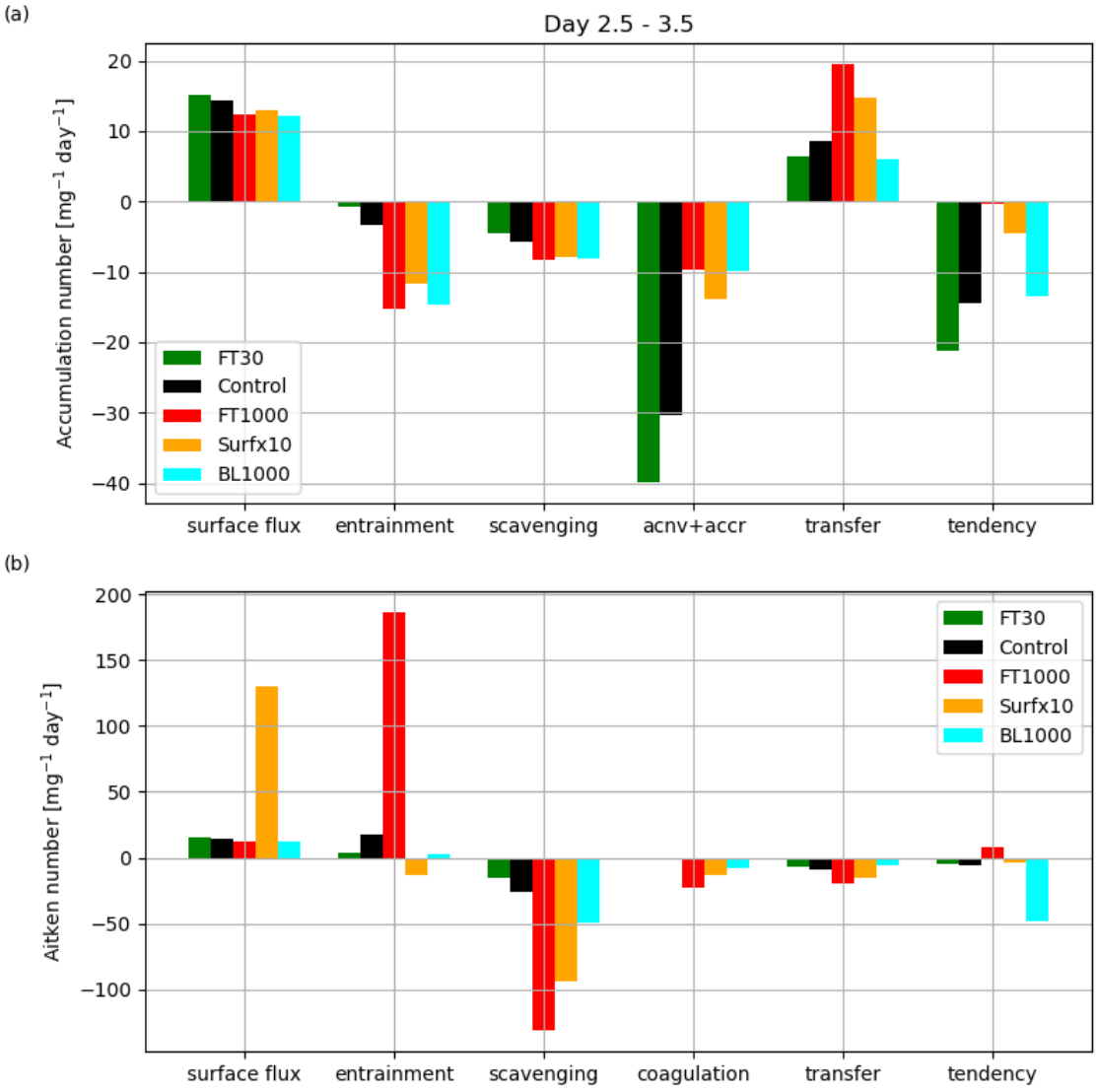

Figure 13. Principal BL-mean number budget terms averaged over days 2.5-3.5 for Control and perturbation experiments for accumulation mode (a) and Aitken mode (b). The scavenging bars represent the scavenging of dry interstitial aerosol by cloud or rain water. The 'acnv+accr' bars are changes due to sum of autoconversion and accretion. The tendency is the total tendency of mean number concentration. Note that the vertical scales differ greatly between (a) and (b).

maintains a lower accumulation mode concentration and therefore higher precipitation-related autoconversion and accretion loss rates of accumulation number than FT1000.

The BL1000 experiment maintains a BL and cloud state similar to FT1000 and Surfx10 during the averaging period of the budget, but both Aitken and accumulation mode aerosol concentrations are decreasing. The Aitken loss is mainly from interstitial scavenging. The accumulation loss is due to similar contributions from entrainment, autoconversion/accretion and Brownian scavenging.

Taken as a group these perturbation experiments show that a significant entrainment-based or surface-based source of Aitken aerosols due to entrainment or surface fluxes can prevent the collapse process in this VOCALS RF06 case by buffering the accumulation mode against precipitation-driven losses. An initial elevated Aitken concentration in BL1000 fades in a few days when these loss processes are not counteracted by a sustained aerosol source from above or from the surface.

4.3 Aerosol Physics Perturbations

We next consider a set of 10-day perturbation experiments, NoScav, NoChem, and WideAit that help explore some underlying processes in the Control run. Figure 14 shows the mean BL evolution of these cases relative to Control.

In NoScav the scavenging of interstitial aerosols is turned off. This prevents BL collapse, with 100% cloud cover and nearly steady LWP during the 10-day simulation. The inversion height lowers very slowly over the last 7 simulation days. The Aitken mode population increases to a steady state concentration of 85 mg^{-1}. The accumulation aerosol population declines very slowly to about 60 mg^{-1} at the end of the simulation. At that time the precipitation rate has grown large enough that the BL collapse feedback could soon occur if the simulation were extended.

The NoChem run has no active chemistry, prenventin growth of aerosol mass through oxidation or H_2SO_4 uptake. The first 2 days of the NoChem run have similar MBL and aerosol properties to the Control run. However the BL accumulation mode aerosol is lost more quickly in NoChem, leading to boundary layer collapse about 14 hours sooner than in Control. After collapse the NoChem and Control runs have broadly similar properties.

The WideAit run specifies a wider $\sigma_g = 1.8$ for Aitken aerosols compared with 1.4 for the Control case. (Note that the parameterization for number flux of Aitken aerosols from the surface is the same as in Control, while the Aitken mass flux increases with the broader mode). There is an immediate depletion of Aitken aerosols in WideAit relative to Control. Otherwise the WideAit simulation tracks the Control case closely for the first 2 or 3 days. Despite the lower Aitken concentrations in the BL, the net transfer to accumulation mode in WideAit is larger than in Control, delaying and slowing the BL collapse. After collapse, WideAit has a higher LWP, higher cloud fraction, and a deeper BL than Control.

The contrast of WideAit with Control is further illustrated in the BL aerosol size distributions at Day 3 (Fig. 15). The wider Aitken distribution overlaps strongly with the accumulation mode distribution, which enables a higher transfer rate of the largest Aitken aerosols and reduces the accumulation modal diameter. This overlapping distribution shape and enhanced aerosol transfer to accumulation mode persists through the BL collapse to the end of the simulation.

The NoChem Aitken distribution is very similar to Control, but because accumulation mode aerosols grow less rapidly without active chemistry, the NoChem accumulation mode has a smaller diameter than Control. Interstitial scavenging of the accumulation mode is more efficient for smaller aerosol sizes, causing the earlier BL collapse in NoChem.

Figure 16 shows horizontal-mean vertical profiles of chemical gas species in Control and aerosol masses for Control and NoChem at selected times (the final Day 5 sounding in each case falls after BL collapse). In Control, the only DMS source is the surface, and DMS is rapidly oxidized by OH in the BL to produce SO_2, so DMS concentration falls off quickly with height. SO_2 is lost primarily through aqueous oxidation in the upper BL by cloud droplets and is also converted to H_2SO_4. H_2SO_4 is almost completely removed in the upper BL by cloud droplets, with smaller losses at a range of heights by aerosol particles. After collapse, when LWP and aerosol concentrations are much reduced, the SO_2 and H_2SO_4 concentrations build up rapidly at most heights in the BL. The peak in H_2SO_4 just above the inversion, prominent in the day 5 sounding, could be a potential site of new particle formation (see Kazil et al. (2011)), though this process is not represented in our model.

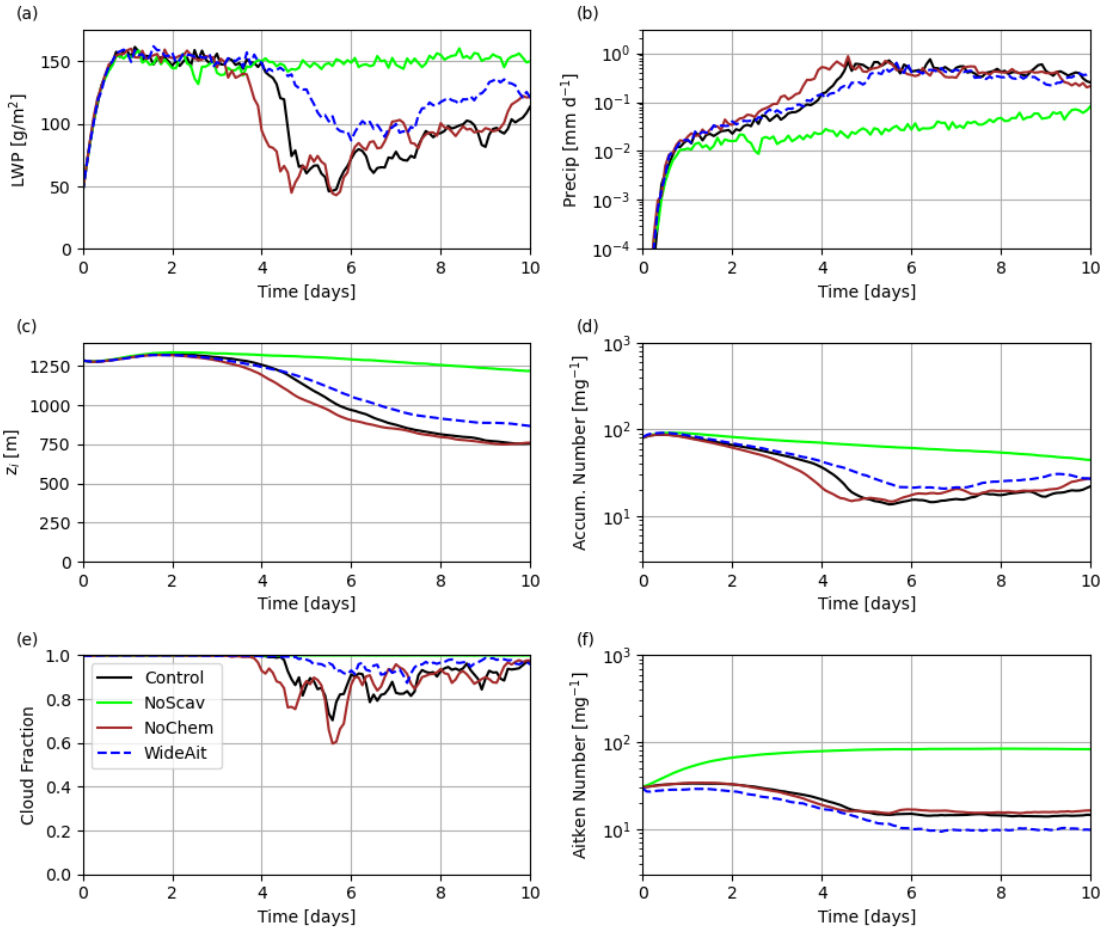

Figure 14. Mean boundary-layer evolution of Control, NoScav, NoChem, and WideAit experiments.

Over time the accumulation aerosol mass in Control is steadily and substantially increased by SO_2 oxidation in cloud, in contrast to an almost constant accumulation-mode aerosol mass in NoChem until BL collapse. This enlarged aerosol mass is connected with the larger size of accumulation aerosols in Control and the delayed collapse relative to NoChem. The Aitken masses are reduced almost identically with time in both Control and NoChem, implying that the chemistry in Control is having minimal influence on the Aitken particles.

5 Discussion and Conclusions

To better simulate and understand the role of Aitken aerosols in the remote MBL, we have a developed a new two-mode aerosol scheme for use in an LES model. The scheme

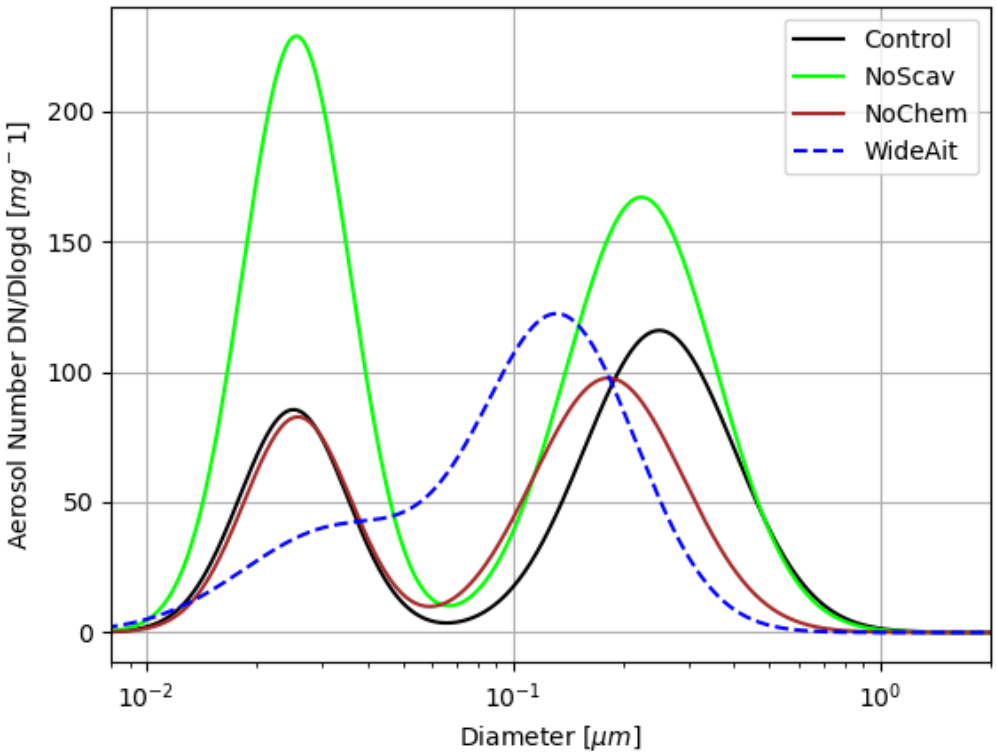

Figure 15. Mean BL aerosol distributions for Control, NoScav, NoChem, and WideAit at Day 3.

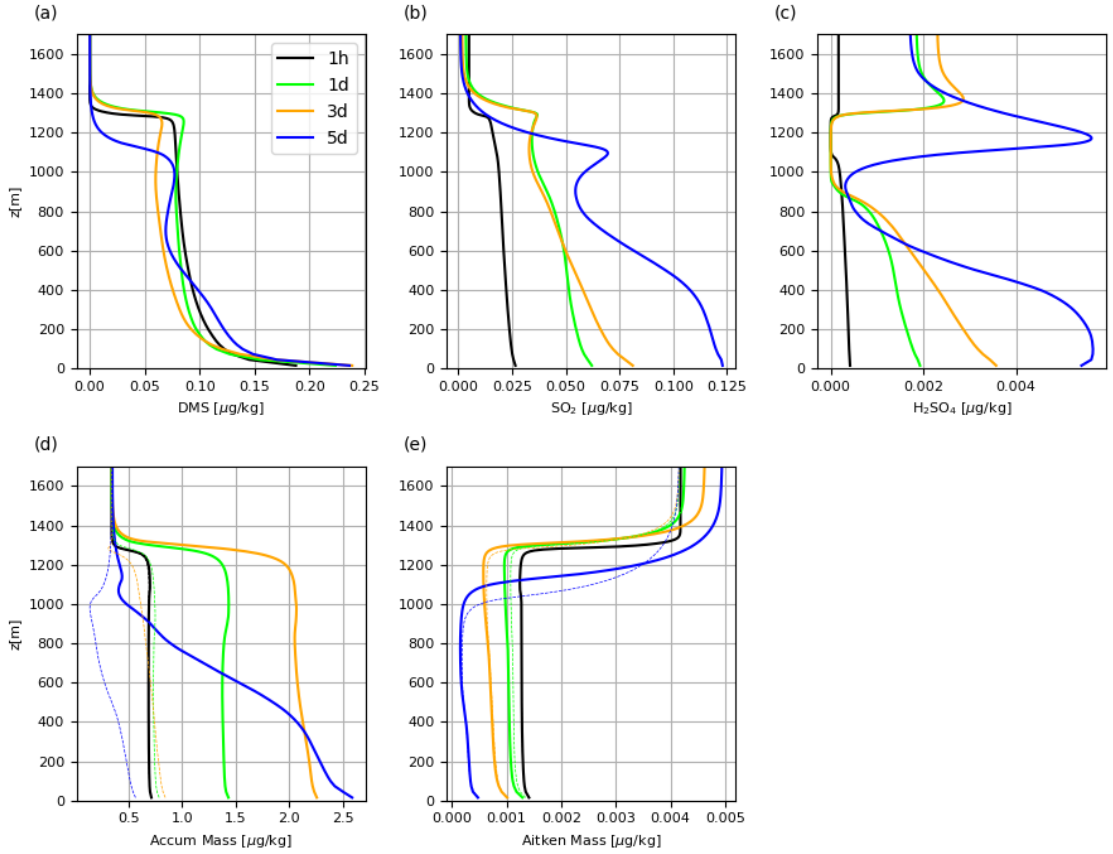

Figure 16. Mean soundings of gas species (a) DMS, (b) SO_2, (c) H_2SO_4, (d) accumulation aerosol mass, and (e) Aitken aerosol mass for the Control experiment (solid). NoChem aerosol masses are plotted in (d) and (e) as thin dashed lines.

requires 7 prognostic variables for aerosol and is designed for use with a bulk two-moment microphysical scheme. The scheme is designed to ensure that most of the small-diameter lognormal 'Aitken' mode consists of aerosol that has never been activated into a cloud droplet, and most of the larger-diameter 'accumulation' mode has been activated and incorporated into a cloud droplet at some time. This structure is maintained by direct transfer from the Aitken to the accumulation mode in saturated updrafts whenever Aitken model aerosols outnumber accumulation mode aerosols for the minimum activated diameter. This assumption acts as an important transfer valve that prevents excessive depletion of the Aitken mode. The aerosols also interact with rudimentary sulfate chemistry appropriate for the remote MBL.

We have demonstrated the new modal scheme using an idealized VOCALS RF06 case where, with default settings, the boundary layer collapses due to steady depletion of accumulation mode aerosols and precipitation feedbacks. Larger Aitken aerosols in the boundary layer slow the collapse by transfer to the accumulation mode. In two sensitivity experiments, FT1000 and Surfx10, additional input of Aitken aerosols from the free troposphere or the sea surface prevents BL collapse by supplying a steady population of accumulation mode aerosols, in support of the Aitken buffering hypothesis of McCoy et al. (2021).

The 8km x 8km domain in these simulations encompasses multiple updrafts and downdrafts and can represent key cloud-aerosol-precipitation feedbacks and sensitivities. However, it is too small to adequately span the mesoscale organization that spontaneously develops in stratocumulus-topped boundary layers, which may modulate the onset of significant surface precipitation and associated wet aerosol scavenging. In test simulations with a 12x16km domain (not shown), the LWP after one day spin-up was slightly larger than in Control, leading to a faster BL collapse. Ideally an even larger domain should be used to capture POC structure and related aerosol feedbacks.

New particle formation, not present in our simulation, could provide a significant source of Aitken particles (Kazil et al., 2011) and is occasionally observed in Southeast Pacific pockets of open cells (Tomlinson et al., 2007; Wood et al., 2008). Including this process would require treatment of more chemical species and processes.

Our scheme assumes aerosol with fixed lognormal shape based on the width parameter σ_g chosen for each mode, so an appropriate σ_g must be chosen for each desired

562 case. The WideAit simulation illustrates that a wider Aitken mode can increase trans-
563 fer to the accumulation mode and affect other aspects of the aerosol size distribution.

564 We plan to test this two-mode scheme in other stratocumulus and shallow cumu-
565 lus settings, especially in cases where Aitken aerosol measurements provide constraints
566 on initial conditions and checks on the simulated aerosol spectrum, such as the recent
567 ACE-ENA experiment (Wang et al., 2021).

568 A Appendix

569 The conservation equations of our two-mode aerosol scheme are modified and ex-
570 tended from the one-mode scheme of B13:

$$\begin{aligned}\dot{N}_{ad} = \dot{N}_{ad}|_{\mathrm{Srf}} - \dot{N}_{ad}|_{\mathrm{Act}} - \dot{N}_{ad}|_{\mathrm{ScvCld}} - \dot{N}_{ad}|_{\mathrm{ScvRn}} + \dot{N}_{c}|_{\mathrm{Evap}} \\ + \dot{N}_{r}|_{\mathrm{Evap}} + \dot{N}_{ait}|_{\mathrm{Trans}} + \dot{N}_{ad}|_{\mathrm{NMT}}\end{aligned} \tag{A.1}$$

$$\dot{N}_{c} = \dot{N}_{ad}|_{\mathrm{Act}} - \dot{N}_{c}|_{\mathrm{Auto}} - \dot{N}_{c}|_{\mathrm{Accr}} - \dot{N}_{c}|_{\mathrm{Evap}} + \dot{N}_{c}|_{\mathrm{NMT}} \tag{A.2}$$

$$\dot{N}_{ait} = \dot{N}_{ait}|_{\mathrm{Srf}} - \dot{N}_{ait}|_{\mathrm{ScvCld}} - \dot{N}_{ait}|_{\mathrm{ScvRn}} - \dot{N}_{ait}|_{\mathrm{Coag}} - \dot{N}_{ait}|_{\mathrm{Trans}} + \dot{N}_{ait}|_{\mathrm{NMT}} \tag{A.3}$$

$$\dot{N}_{r} = \dot{N}_{c}|_{\mathrm{Auto}} - \dot{N}_{r}|_{\mathrm{SlfC}} - \dot{N}_{r}|_{\mathrm{Evap}} - \dot{N}_{r}|_{\mathrm{Fallout}} + \dot{N}_{r}|_{\mathrm{NMT}} \tag{A.4}$$

$$\begin{aligned}\dot{q}_{acc} = \dot{q}_{acc}|_{\mathrm{Srf}} - \dot{q}_{acc}|_{\mathrm{Auto}} - \dot{q}_{acc}|_{\mathrm{Accr}} - \dot{q}_{acc}|_{\mathrm{ScvRn}} + \dot{q}_{ait}|_{\mathrm{ScvCld}} + \dot{q}_{acc}|_{\mathrm{Coag}} + \dot{q}_{ar}|_{\mathrm{Evap}} \\ + \dot{q}_{acc}|_{\mathrm{SO_2ox}} + \dot{q}_{acc}|_{\mathrm{Uptk}} + \dot{q}_{ait}|_{\mathrm{Trans}} + \dot{q}_{acc}|_{\mathrm{NMT}}\end{aligned} \tag{A.5}$$

$$\dot{q}_{ait} = \dot{q}_{ait}|_{\mathrm{Srf}} - \dot{q}_{ait}|_{\mathrm{ScvCld}} - \dot{q}_{ait}|_{\mathrm{ScvRn}} - \dot{q}_{ad}|_{\mathrm{Coag}} + \dot{q}_{ait}|_{\mathrm{Uptk}} - \dot{q}_{ait}|_{\mathrm{Trans}} + \dot{q}_{ait}|_{\mathrm{NMT}} \tag{A.6}$$

$$\dot{q}_{ar} = \dot{q}_{acc}|_{\text{Auto}} + \dot{q}_{acc}|_{\text{Accr}} + \dot{q}_{acc}|_{\text{ScvRn}} + \dot{q}_{ait}|_{\text{ScvRn}} - \dot{q}_{ar}|_{\text{Evap}} - \dot{q}_{ar}|_{\text{Fallout}} + \dot{q}_{ar}|_{\text{NMT}} \tag{A.7}$$

Three processes conserve aerosol number and mass: activation of aerosols into cloud droplets (Act), evaporation of cloud droplets and rain (Evap) and transfer of Aitken to accumulation mode (Trans). Six processes destroy aerosol number while conserving aerosol mass: scavenging of interstitial aerosol by cloud and rain (ScvCld and ScvRain, respectively), autoconversion and accretion of cloud water (Auto and Accr, respectively), self-collection of rain drops (SlfC), and coagulation (Coag). Two chemical processes, oxidation of SO_2 in cloud drops (SO_2ox) and uptake of gaseous H_2SO_4 within cloud droplets (Uptk), modify aerosol mass but not aerosol number. Surface fluxes (Srf) act as sources for both aerosol mass and number, and NMT terms represent terms associated with non-microphysical processes (advection, large-scale subsidence, and sub-grid scale turbulence).

Equation A.1 for $\dot{N}_{ad}$ is the same as in B13 except for an additional term representing transfer from the Aitken mode. Equations A.2, A.4 are identical to equations in B13. Equations A.3 and A.6 are new equations for Aitken number and mass. Equation A.5 for $\dot{q}_{acc}$ has new terms for coagulation, Aitken transfer, SO_2 oxidation (Equation (6)), and uptake (Equation (7)). The Aitken transfer rate terms for number and mass are calculated numerically using the technique described in Section 2.1. Equation A.7 for $\dot{q}_{ar}$ adds a term to B13 representing scavenging of Aitken aerosol by rain water. All scavenging terms are computed using the scheme described in B13. Surface flux terms use Equations (1) and (2). Autoconversion, accretion, self-collection, evaporation, and fallout terms are determined in the microphysics scheme of Morrison and Grabowski (2008). Coagulation terms come from Binkowski and Shankar (1995).

Acknowledgments

We acknowledge funding from the U. S. Department of Energy Atmospheric System Research program under grant DE-SC0020134. PNB acknowledges support from Lowercarbon, the Pritzker Innovation Fund and SilverLining through the Marine Cloud Brightening Project. Research by ILM is supported by the NOAA Climate and Global Change Postdoctoral Fellowship Program, administered by UCAR's Cooperative Programs for

the Advancement of Earth System Science (CPAESS) under award NA18NWS4620043B. We thank Marat Khairoutdinov for maintaining SAM and enabling its support of different microphysical schemes. We also thank Becky Alexander and Joel Thornton for useful conversations.

The SAM model inputs and important model outputs presented in this paper and the SAM source code for the modal aerosol model described will be archived at

https://doi.org/10.5281/zenodo.5746102.

References

Abdul-Razzak, H., and Ghan, S. J. (2000). A paramterization of aerosol activation: 2. Multiple aerosol types. *J. Geophys. Res.*, *105*, 6837-6844.

Allen, G., and 38 co-authors (2011). South East Pacific atmospheric composition and variability sampled along 20° S during VOCALS-REx. *Atmos. Chem. and Phys.*, *11*, 5237–5262. https://doi.org/10.5194/acp-11-5237-2011

Berner, A. H., Bretherton, C. S., Wood, R., and Muhlbauer, A. (2013). Marine boundary layer cloud regimes and POC formation in a CRM coupled to a bulk aerosol scheme. *Atmospheric Chemistry and Physics*, *13*, 12549–12572. https://doi.org/10.5194/acp-13-12549-2013

Bey, I., Jacob, D. J., Yantosca, R. M., Logan, J. A., Field, B., Fiore, A. M., Li, Q., Liu, H., Mickley, L. J., and Schultz, M. (2001) Global modeling of tropospheric chemistry with assimilated meteorology: Model desctiption and evaluation. *J. Geophys. Res.*, *106*, 23073–23096.

Binkowski, F. S., and U. Shankar (1995) The Regional particulate matter model. 1. Model description and preliminary results. *J. Geophys. Res.*, *100*, 26191–26209.

Clarke, A. D., Owens, S. R., and Zhou, J. (2006) An ultrafine sea-salt flux from breaking waves: Implications for cloud condenstation nuclei in the remote marine atmosphere. *J. Geophys. Res.*, *111*, 1–14. https://doi.org/10.1029/2005/JD006565

Covert, D. S., Kapustin, V. N., Bates, T. S., and Quinn, P. K. (1996) Physical properties of marine boundary layer aerosol particles of the mid-Pacific in relation to sources and meterological transport. *J. Geophys. Res.*, *101.D3*, 6919–6930. https://doi.org/10.1029/95JD03068

Durkee, P. A., Noone, K. J., Ferek, R. J., Johnson, D. W., Taylor, J. P., Garrett, T. J., Hobbs, P. V., Hudson, J. G., Bretherton, C. S., Innis, G., Frick, G. M., Hoppel, W. A., O'Dowd, C. D., Russell, L. M., Gasparovic, R., Nielsen, K. E., Tessmer, S. A., Öström, E., Osborne, S. R., Flagan, R. C., Seinfeld, J. H., and Rand, H. (2000) The impact of ship-produced aerosols on the microstructure and albedo of warm marine stratocumulus clouds: a test of MAST hypothesis 1i and 1ii. *J. Atmos. Sci.*, *57*, 2254–2569, https://doi.org/10.1175/1520-0469(2000)057

Ekman, A. M., Wang, C., Ström, and Krejci, R. (2006) Explicit simulation of aerosol physics in a cloud-resolving model: aerosol transport and processing in the free troposphere. *J. Atmos. Sci*, *63*, 682–696. https://doi.org/10.1175/JAS3645.1

Flossmann, A. I., Hall, W. D., and Pruppacher, H. R. (1985). theoretical study of the wet removal of atmospheric pollutants. Part I: The redistribution of aerosol particles captured through nucleation and impaction scavenging by growing cloud drops. *J. Atmos. Sci.*, *42*, 583–606, https://doi.org/10;1175/1520-0469(1985)042¡0583:ATSOTW¿2.0.CO;2

Hoppel, W. A., Fitzgerald, J. W., Frick, G. M., Larson, R. E., and Mack, E. J. (2000). Aerosol size distributions and optical properties found in the marine boundary layer over the Atlantic Ocean. *J. Geophys. Res. Atmos.*, *95*, 3659–3686, https://doi.org/10.1029/JD095iD04p03659

Ivanova, I. T., and Leighton, H. G. (2008). Aerosol-cloud interactions in a mesoscale model. Part I: Sensitivity to activation and collision-coalescence. *J. Atmos. Sci.*, *65*, 289–308, https://doi.org/10.1175/2007JAS2207.1

Kazil., J., Wang, H., Feingold, G., Clarke, A. D., Snider, J. R., and Bandy, A. R. (2011). Modeling chemical and aerosol processes in the transition from closed to open cells during VOCALS-REx. *Atmos. Chem. Phys.*, *11*, 7491–7514, https://doi.org/10.5194/acp-11-7491-2011

Khairoutdinov, M. F., and Randall, D. A. (2003). Cloud resolving modeling of the ARM summer 1997 IOP: Model formulation, results, uncertainties, and sensitivities. *J. Atmos. Sci.*, *60*, 607–625.

Liu, X., and coauthors (2012). Toward a minimal representation of aerosols in climate models: description and evaluation in the Community Atmosphere Model

CAM5. *Geosci. Model Dev.*, *5*, 709–739, https://doi.org/10.5194/gmd-5-709-2012

McCoy, D. T., Bender, F. A. M., Grosvenor, D. P., Mohrmann, J. K., Hartmann, D. L., Wood, R., and Field, P. R. (2018). Predicting decadal trends in cloud droplet number concentration using reanalysis and satellite data. *Atmos. Chem. Phys.*, *18*, 2035–2047.

McCoy, I. L., McCoy, D. T., Wood, R., Regayre, L., Watson-Parris, D., and Grosvenor, D. P. (2020). The hemispheric contrast in cloud microphysical properties constrains aerosol forcing. *Proc. Natl. Acad. Sci. USA*, *117*, 18998–19006. https://www.ncbi.nlm.nih.gov/pubmed/32719114

McCoy, I .L., Bretherton, C. S., Wood, R., Twohy, C. H., Gettelman, A., Bardeen, C. G., and Toohey, D. W. (2021). Influences of recent particle formation on Southern Ocean aerosol variability and low cloud properties. *J. Geophys. Res. Atmos.*, *126*, https://doi.org/10.1029/2020JD033529

Mlawer, E. J., Taubman, S. J., Brown, P. D., Iacono, M. J., and Clough, S. A. (1997). Radiative tranfer for inhomogeneous atmospheres: RRTM, a validated correlated-k model for the longwave. *J. Geophys. Res.*, *102*, 16663–16682, https://doi.org/10.1029/97JD00237

Morrison, H. and Grabowski, W. W. (2008). Modeling supersaturation and subgrid-scale mixing with two-moment bulk warm microphysics. *J. Atmos. Sci.*, *65*, 792–812, https://doi.org/10.1175/2007JAS2374.1

Nightingale, P. D., Malin, G., Law, C. S., Watson, A. J., Liss, P. S, Liddicoat, M. I., Boutin, J., Upstill-Goddard, R. C. (1999). In situ evaluation of air-sea gas exchange parameterizations using novel conservative and volatile tracers. *Glob. Biogeochem. Cyc.*, *14*, 373–387.

Ovcninnikov, M., and Easter, R. C. (2010). Modeling aerosol growth by aqueous chemistry in a nonprecipitating stratiform cloud. *J. Geophys. Res.*, *115*, D14210. https://doi.org/doi:10.1029/2009JD012816

Quinn, P., Coffman, D., Johnson, J., Upchurch, L. M., and Bates, T. S. (2017). Small fraction of marine cloud condensation nuclei made up of sea spray aerosol. *Nature Geosci.*, *10*, 674–679. https://doi.org/10.1038/ngeo3003

Raes, F. (1995). Entrainment of free tropospheric aerosols as a regulating mechanism for cloud condensation nuclei in the remote marine boundary layer. *J.*

Geophys. Res., *100.D2*, 2893–2903.

Sanchez, K. J., Chen, C. L., Russell, L. M., Betha, R., Liu, J., and Price, D. J. (2018). Substantial seasonal contribution of observed biogenic sulfate particles to cloud condensation nuclei. *Sci. Reports*, *8(1)*, 3235. https://www.ncbi.nlm.nih.gov/pubmed/29459666

Tomlinson, J. M., Li, R., and Collins, D. R. (2007). Physical and chemical properties of the aerosol within the southeastern Pacific marine boundary layer. *J. Geophys. Res.*, *112.D2* https://doi.org/10.1029/2006JD007771

Tonttila, J., Maalick, Z., Raatikainen, T., Kokkola, H., Kühn, T., and Romakkaniemi, S. (2017). UCLALES-SALSA v1.0: a large-eddy model with interactive sectional microphysics for aerosol, clouds, and precipitation. *Geosci. Model Dev.*, *10*, 169–188. https://doi.org/10.5194/gmd-10-169-2017

Platnick, S. and Twomey, S. (1994). Determining the susceptibility of cloud albedo to changes in droplet concentration with the advanced very high resolution radiometer. *J. Appl. Meteor.*, *33*, 334–347, https://doi.org/10.1175/1520-0450(1994)033¡0334:DTSOCA¿2.0.CO;2

Wang, J. and co-authors (2021). Aerosol and Cloud Experiments in the Eastern North Atlantic (ACE-ENA). Accepted for publication in *Bull. Amer. Meteor. Soc*

Whitby, E. R., McMurry, P. H., Shankar, U., and Binkowski, F. S. (1991). Modal aerosol dynamics modeling. *Rep. 600/3-91/020*, Atmos.Res. and Exposure Assess. Lab., U.S. Environ. Prot. Agency, Research Triangle Park, NC, 1991. (Available as PB91-161729/AS from Natl. Tech. Inf. Serv., Springfield VA.

Wood, R., Comstock, K. K., Bretherton, C. S., Cornish, C., Tomlinson, J., Collins, D. R., and Fairall, C. (2008) Open cellular structure in marine stratocumulus sheets. *J. Geophys. Res.*, *113*. https://doi.org/10.1029/2007JD009371

Wood, R., Bretherton, C. S., Leon, D., Clarke, A. D., Zuidema, P., Allen, G., and Coe, H. (2011). *Atmos. Chem. Phys.*, *11*, 2341–2370., https://doi.org/10.5194/acp-11-2341-2011

Wyant, M. C., Bretherton, C. S., Wood, R., Carmichael, G. R., Clarke, A., Fast, J., George, R., Gustafson Jr., W. I., Hannay, C., Lauer, A., Lin., Y., Morcrette, J.-J., Mulcahy, J., Saide, P. E., Spak, S. N., and Yang, Q. (2015). Global and regional modeling of clouds and aerosols in the marine boundary layer

during VOCALS: the VOCA intercomparison. *Atmos. Chem. and Physics*, *15*, 153-172, https://doi.org/10.5194/acp-15-153-2015

Yamaguchi, T., Randall, D. A., and Khairoutdinov, M. F. (2011). *Mon. Weather Rev.*, *139*, 3248-3264.

Zaveri, R. .A., Easter, R. C., Fast, J. D., and Peters, L. K. (2008). Model for simulating aerosol interactions and chemistry (MOSAIC). *J. Geophys. Res.*, *113*, D13204 https://doi.org/10.1029/2007JD008782

Zheng, G., Wang, Y., Aiken, A. C., Gallo, F., Jensen, M. P., Kollias, P., Kuang, C., Luke, E., Springston, S., Uin, J., Wood. R., and Wang., J. (2018). Marine boundary layer aerosol in the eastern North Atlantic: seasonal variations and key controlling processes. *Atmos. Chem. and Phys.*, *18(23)*, 17615–17635. https://doi.org/10.5194/acp-18-17615-2018

Zieger, P., Väisänen, O., Corbin, J. C., Partridge, D. G., Bastelberger, S., Mousavi-Fard, M., Rosati, B., Gysel, M., Krieger, U. K., Leck, C., Nenes, A., Riipinen, I., Virtanen, A., and Salter, M. E. (2017). Revising the hygroscopicity of inorganic sea salt particles. *Nat. Commun.*, *8*, 15583, https://doi.org/10.1038/ncomms15583